

Domain formation in cholesterol–phospholipid membranes exposed to adhesive surfaces or environments†

Cite this: *Soft Matter*, 2013, **9**, 8438

Reinhard Lipowsky,^{*a} Tahereh Rouhiparkouhi,^a Dennis E. Discher^b and Thomas R. Weikel^a

Domain formation in binary mixtures of cholesterol and a single phospholipid has been studied for a long time but the nature of these domains is still a matter of some debate. One interpretation of these domains is that they arise from the coexistence of liquid-ordered and liquid-disordered phases within the membranes. Here, we study the effect of adhesive surfaces and environments on the proposed phase behavior theoretically. The adhesion or partial support of the membranes leads to two or several membrane segments that exhibit different molecular interactions with their environments and, thus, have different molecular affinities to these environments. We show that the affinity contrasts between different environments strongly affect the phase behavior of the membranes. First, the affinity contrasts confine the domain formation spatially to single membrane segments. Second, these contrasts lead to a partitioning of the coexistence region in the composition–temperature plane into distinct coexistence regions for the different membrane segments. Third, the range of membrane compositions, for which one can observe domain formation in one of the membrane segments, is always reduced compared to the composition range of the free membrane. Furthermore, small affinity contrasts represent singular perturbations in the sense that the phase diagrams change in a discontinuous manner as one varies the affinity contrast from small positive to small negative values. All of these results are quite general because they follow from thermodynamic stability alone and apply to any two-component membrane with fluid–fluid coexistence. In addition to these generic features, we also provide a computational scheme, by which one can explicitly calculate the partitioning of the coexistence regions for a specific binary mixture, and illustrate this scheme for binary cholesterol–DPPC membranes. Both the generic and the specific features of domain formation as predicted by our theory are accessible to experimental studies.

Received 12th March 2013

Accepted 25th June 2013

DOI: 10.1039/c3sm50712b

www.rsc.org/softmatter

1 Introduction

A lot of experimental effort has been devoted to the phase behavior of lipid membranes containing a binary cholesterol–phospholipid mixture.^{1–10} Based on spectroscopic methods, calorimetry, and freeze fracture electron microscopy, a variety of phases have been distinguished and different phase diagrams have been proposed. Here, we will be primarily concerned with the possible coexistence of two fluid phases, as recently reviewed in ref. 11. Such a fluid–fluid coexistence implies the formation of two different types of fluid domains within the membranes.

About thirty years ago, electron spin resonance (ESR) data provided some evidence that the phase diagram of cholesterol–DMPC bilayer membranes contains a region, in which two different types of fluid domains may coexist.³ Somewhat later, such a coexistence region was also found for cholesterol–DPPC mixtures using deuterium nuclear magnetic resonance (NMR)^{4,5,10} as well as ESR.⁶ The NMR data were interpreted in terms of phase separation into two fluid phases, denoted as liquid-ordered and liquid-disordered phases.¹²

This interpretation has remained somewhat controversial, however, since two other mechanisms for the observed domain formation have been proposed: the formation of cholesterol–phospholipid complexes within a single phase¹³ as well as composition fluctuations governed by a large correlation length.^{7–9} In fact, two recent experimental studies^{9,10} that applied deuterium NMR to the ternary cholesterol–DPPC–DOPC mixtures came to different conclusions about the phase behavior of binary cholesterol–DPPC mixtures. The ternary phase diagram can be visualized as a Gibbs prism that is spanned by the temperature axis and the mole fractions of the

^aTheory & Biosystems, Max Planck Institute of Colloids and Interfaces, 14424 Potsdam, Germany. E-mail: lipowsky@mpikg.mpg.de; Fax: +49 331 5679602; Tel: +49 331 5679600

^bBiophysical Engineering, University of Pennsylvania, Philadelphia, PA 19104, USA

† Electronic supplementary information (ESI) available: Two appendices on (i) composition of spectator phases and (ii) chemical equilibrium between many membrane segments. See DOI: 10.1039/c3sm50712b

three components that form a Gibbs triangle. The three side faces of this Gibbs prism correspond to the partial phase diagrams for the binary mixtures cholesterol–DPPC, cholesterol–DOPC and DPPC–DOPC, respectively. Whereas Veatch *et al.*⁹ concluded that the partial phase diagram for cholesterol–DPPC does *not* contain a fluid–fluid coexistence region of liquid-ordered and liquid-disordered phases, Davis *et al.*¹⁰ came to precisely the opposite conclusion.

In view of this controversy, it is useful to explore possible consequences of the proposed fluid–fluid coexistence of cholesterol–phospholipid mixtures. In the present paper, we show theoretically that such a phase behavior is strongly affected by adhesive environments as provided, *e.g.*, by other membranes or surfaces. Indeed, these environments strongly affect both the spatial organization and the composition of intramembrane domains. One example is provided by the adhesion of vesicles as shown in Fig. 1.

In the left column of this figure, we see freely suspended vesicles with different compositions. The membranes of these vesicles are exposed to a single, uniform environment, corresponding to the two aqueous solutions on both sides of the membranes. In the following, such membranes that are freely suspended and fully hydrated in aqueous solution will be denoted as “free membranes”.

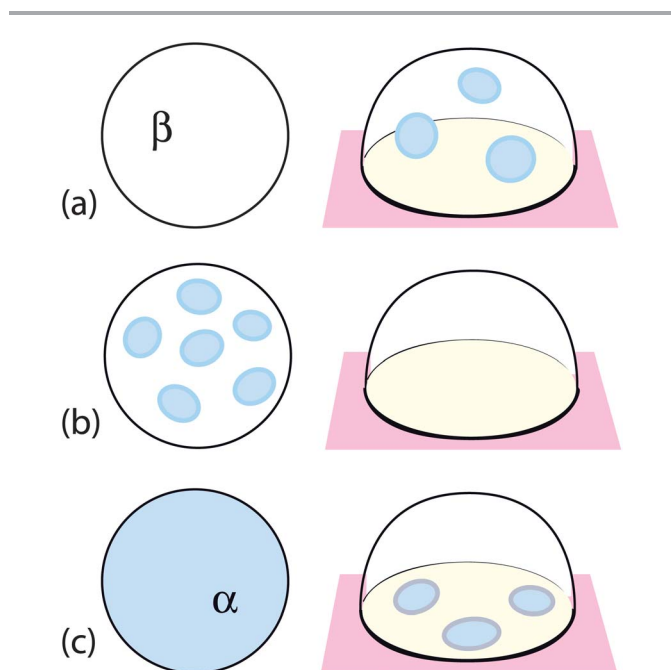


Fig. 1 (Left column) Domain patterns of free vesicle membranes consisting of a cholesterol–phospholipid mixture that undergoes phase separation into a liquid-ordered phase α (blue) and a liquid-disordered phase β (white). (Right column) The same vesicles in contact with an adhesive surface that attracts the phospholipids more strongly than cholesterol. The rows (a), (b), and (c) correspond to low, intermediate, and high cholesterol concentrations, respectively. In (a), the surface induces intramembrane domains only in the unbound membrane segment (white/blue); in (b), domain formation is completely suppressed by the surface; and in (c), the surface-induced domain formation is restricted to the bound membrane segment (yellow/blue). The multi-domain patterns shown here correspond to the early stages of phase separation.

In the right column of Fig. 1, we see the same vesicles but now in contact with an adhesive substrate surface that could be provided by a solid substrate or another membrane. For such an adhesion geometry, the membrane consists of two segments that are exposed to two different environments. The unbound membrane segment far away from the surface experiences the same environment and, thus, the same molecular interactions as the free membrane in the absence of the surface. In contrast, the bound membrane segment in close contact with the surface experiences different molecular interactions arising from the adhesive surface. As previously described in ref. 14, pore- or hole-spanning membranes as well as membranes adhering to chemically patterned surfaces provide further examples for membranes exposed to two different environments.

The ESR and NMR methods, which revealed domain formation in binary cholesterol–phospholipid mixtures, did not provide information about the *size* of these domains. In addition, it has not been possible, so far, to detect these domains by fluorescence microscopy. Phase separation will initially lead to multi-domain patterns as displayed in Fig. 1. The line tension of the domain boundaries will then favor the coalescence of small domains into larger ones.^{15,16} However, even the equilibrium pattern may consist of more than two domains if the two phases have sufficiently different bending rigidities.¹⁷

In general, any membrane environment will attract the two molecular components, here cholesterol and a phospholipid species, with different affinities, *i.e.*, any such environment has the tendency to recruit certain components and to expel others. Therefore, two different environments will partition the membrane into two segments that differ in their composition. As shown below, this membrane partitioning arising from the affinity contrast between the environments strongly affects the phase diagram of the binary mixture. Indeed, we find that the single fluid–fluid coexistence region for the free membrane is replaced by two fluid–fluid coexistence regions for the two membrane segments.

This phase behavior has important consequences for the formation of intramembrane domains. Thus, depending on the cholesterol concentration, domains may only form in one of the two membrane segments as shown in Fig. 1(a) and (c) but not in both segments simultaneously. Furthermore, the segmentation of the membrane by two environments may completely suppress the intramembrane domains that were present in the free membrane, see Fig. 1(b). In all cases, the composition of the intramembrane domains in the two membrane segments differs from the composition of the domains within the free vesicle membrane.

The theory described here is based on thermodynamics and generalizes our previous study of the lattice binary mixture or Ising model¹⁴ to any two-component membrane that exhibits a fluid–fluid coexistence region. In particular, we do not have to make any assumptions about the shape of this coexistence region because we take the experimentally determined phase diagram of the free membrane explicitly into account.

Our theory predicts that any two-component membrane, when exposed to two different environments, can only exhibit three distinct domain patterns as shown in the right column of

Fig. 1. Furthermore, the theory enables us to determine the phase diagram for such a membrane in a semi-quantitative manner. In order to do so, we need (i) the phase diagram of the free membrane, (ii) one geometric parameter that determines the area fractions of the two membrane segments, as well as (iii) the affinity contrast between the two environments which is defined in terms of their molecular interactions. As shown below, *any nonzero affinity contrast partitions the coexistence region of the free membrane into two distinct coexistence regions* and, thus, has a rather strong effect on the phase diagram. Furthermore, small affinity contrasts turn out to be singular perturbations because this partitioning changes abruptly as one varies the affinity contrast from small positive to small negative values.

As a specific example, we will discuss the binary mixture of cholesterol and DPPC, for which fluid–fluid coexistence has been deduced from several spectroscopic experiments.^{5,6,10,11} We will start from the corresponding phase diagram and will then consider situations, in which the membranes are exposed to two different environments as in Fig. 1. Our theory can be extended to an arbitrary number of different environments. In the presence of M different environments, the coexistence region of the free membrane is partitioned into M distinct coexistence regions as briefly described at the end of this paper.

Membranes exposed to adhesive surfaces or environments as in Fig. 1 acquire a tension that reflects the balance between the attraction towards the adhesive substrate and the osmotic pressure difference between the interior and exterior compartments of the vesicle.^{18,19} Such a tension may also affect the phase diagram of the membranes. For free membranes, the effect of tension on the phase behavior was theoretically studied for binary mixtures using a local density functional for the composition field.²⁰ For ternary mixtures consisting of cholesterol and two different lipids, this effect was also investigated experimentally.^{21–23} In such experimental studies, the membrane tension should be small compared to the tension of rupture, which is of the order of a few nN m^{-1} . We will argue below that such tensions should have a rather weak effect on the phase diagram, in agreement with the experimental study in ref. 23. As a consequence, the drastic changes of the phase diagram arising from different adhesive environments as described here will be easy to distinguish from any tension-induced changes.

The paper is organized as follows. The phase diagram of freely suspended membranes consisting of cholesterol and a single phospholipid depends on temperature and on the cholesterol's mole fraction, as briefly reviewed in Section 2. This section also discusses the dependence of the phase behavior on membrane tension. The theoretical description for free membranes is explained in some detail in Section 3 and then extended to membranes exposed to two different environments in Sections 4 and 5. The latter section describes the phase behavior as a function of composition and temperature, which both can be controlled experimentally. In Section 6, we apply our general theory to derive phase diagrams for cholesterol–DPPC membranes exposed to adhesive surfaces or environments. We then generalize our results to an arbitrary number of different environments in Section 7, discuss the effect of environments with quenched disorder in Section 8, and give a summary and outlook at the end of the paper.

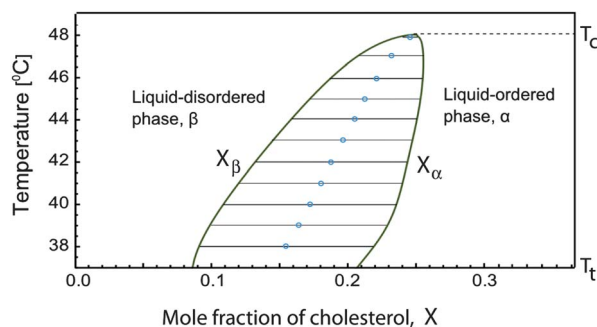


Fig. 2 Experimental phase diagram for binary cholesterol–DPPC membranes deduced from deuterium NMR in ref. 5 and 10 and reviewed in ref. 11, as a function of cholesterol's mole fraction X and temperature T . The fluid–fluid coexistence region between the liquid-ordered phase α on the right and the liquid-disordered phase β on the left is bounded by the two binodal lines $X = X_\beta(T)$ and $X = X_\alpha(T)$, which meet at the critical point with $T = T_c$. The horizontal lines represent tie lines, the blue circles the midpoints of these tie lines, and the triple point temperature $T = T_t$ corresponds to the lowest temperature displayed in this diagram.

2 Phase behavior of free membranes

2.1 Phase diagram of free membranes

As mentioned, we use the term “free membrane” for a freely suspended and fully hydrated membrane exposed to aqueous solutions on both sides. If such a membrane has two components, its phase diagram depends on the ambient temperature T and on the membrane composition. The two membrane components, provided here by cholesterol and a certain phospholipid, will now be denoted by a and b , respectively. The membrane composition is then described by the mole fractions

$$X_a \equiv \frac{\mathcal{N}_a}{\mathcal{N}_a + \mathcal{N}_b} = \frac{\mathcal{N}_a}{\mathcal{N}} \quad \text{and} \quad X_b \equiv \frac{\mathcal{N}_b}{\mathcal{N}} = 1 - X_a \quad (1)$$

where \mathcal{N}_a and \mathcal{N}_b are the molecular numbers and $\mathcal{N} \equiv \mathcal{N}_a + \mathcal{N}_b$.[‡] In order to simplify the notation, we will now omit the subscript a and denote the mole fraction of cholesterol simply by X .

The phase diagram of a free, two-component membrane is then determined by two variables, namely cholesterol's mole fraction X and temperature T , see Fig. 2. This figure displays the fluid–fluid coexistence region for the binary cholesterol–DPPC mixture as experimentally deduced in ref. 5, 6 and 10 and reviewed in ref. 11. As mentioned in the Introduction, we take this phase diagram as a specific example. However, our theoretical approach can be applied to the phase diagram of any binary mixture and, in particular, to the various cholesterol–phospholipid mixtures reviewed in ref. 11.

For the cholesterol–DPPC mixture, the fluid–fluid coexistence region was reported to lie within the temperature range $T_t < T < T_c$ with the triple point temperature $T = T_t \approx 37.5^\circ\text{C}$ and the critical temperature $T = T_c \approx 46^\circ\text{C}$. In this temperature range, the two-component membranes were proposed to attain two different fluid phases, the liquid-ordered phase α , which is rich in cholesterol, and the liquid-disordered phase β , which is

[‡] Calligraphic symbols are used in this paper to denote *extensive* thermodynamic variables such as molecular number \mathcal{N} , area \mathcal{A} , and free energy \mathcal{F} .

poor in cholesterol. The two one-phase regions are separated by the $\alpha\beta$ coexistence region, in which the membrane undergoes phase separation *via* the formation of intramembrane domains. This coexistence region is described by

$$X_\beta(T) \leq X \leq X_\alpha(T) \quad (2)$$

with the two binodal lines

$$X = X_\beta(T) \text{ and } X = X_\alpha(T) \text{ for } T_t < T \leq T_c. \quad (3)$$

It is also useful to consider the width

$$\Delta X(T) = X_\alpha(T) - X_\beta(T). \quad (4)$$

of the coexistence region, which represents the length of the tie lines, as well as the midpoints of these tie lines, see Fig. 2. The curve through these midpoints defines the midline $X_{\text{ml}}(T) = \frac{1}{2}[X_\alpha(T) + X_\beta(T)]$, which is a bisecting arc of the coexistence region and ends in the critical point. As one approaches the critical point at $T = T_c$ from below, the width of the coexistence region vanishes and exhibits the power law behavior $\Delta X(T) \sim |T - T_c|^{1/8}$ corresponding to the universality class of the two-dimensional Ising model.¹⁵

2.2 Dependence of phase behavior on membrane tension

If the freely suspended membrane is stretched by an appreciable tension $\Sigma > 0$, the membrane area is increased from \mathcal{A} to $\mathcal{A} + \Delta\mathcal{A}$. The tension Σ and the relative area change $\Delta\mathcal{A}/\mathcal{A}$ are then related *via* $\Sigma = k_A \Delta\mathcal{A}/\mathcal{A}$ with the area compressibility (or area stretch) modulus k_A . For simplicity, we ignore the entropic tension contribution related to the flattening of membrane undulations. The increase in membrane area implies that the average separation d between the membrane molecules increases as

$$\frac{\Delta d}{d} = \frac{\Sigma}{2k_A}. \quad (5)$$

The area compressibility modulus k_A is of the order of 200 Nm m^{-1} for one-component phospholipid membranes²⁴ and increases with cholesterol content.²⁵ Using the value $k_A = 200$ Nm m^{-1} in eqn (5), we obtain the linear stretch $\Delta d/d \approx 2.5 \times 10^{-4}$ for $\Sigma = 0.1$ mN m^{-1} and $\Delta d/d \approx 2.5 \times 10^{-3}$ for $\Sigma = 1$ mN m^{-1} .

Since the molecules are moved further apart, their long-ranged molecular interactions decreases. For two molecular species a and b as considered here, we have three different pairs of molecules and, thus, three different interaction energies U_{aa} , U_{bb} , and U_{ab} . All molecules interact *via* van der Waals forces with interaction energies U_{ij}^{vdW} that decay as $1/d^6$ with the intermolecular separation d . When this separation is increased from d to $d + \Delta d$, the amplitudes of the interaction energies U_{ij}^{vdW} are reduced by the factor

$$\zeta_\Sigma = 1 - 6 \frac{\Delta d}{d} = 1 - \frac{3\Sigma}{k_A} \quad (6)$$

Using again the value $k_A = 200$ Nm m^{-1} for the compressibility modulus k_A , we obtain the reduction factors $\zeta_\Sigma = 0.9985$ for $\Sigma = 0.1$ mN m^{-1} and $\zeta_\Sigma = 0.985$ for $\Sigma = 1$ mN m^{-1} .

The effect of these reduced interaction energies on the phase diagram can be estimated using a simple but instructive model for two-component membranes, the lattice binary mixture, or the equivalent Ising model.^{14,16,17} In the context of membranes, this lattice model was originally used to study domain formation within adhering membrane segments.^{26,27} Of course, fluid membranes as considered here do not exhibit long-range translational order but the lattice is nevertheless useful in order to incorporate the short-ranged repulsive interactions between the molecules arising from their mutual exclusion whereas the longer-ranged molecular interactions are described by the interaction energies U_{aa} , U_{bb} , and U_{ab} . We use the sign convention that attractive interactions are described by *negative* values of U_{ij} . In the lattice binary mixture, the phase diagram depends only on the reduced temperature T/T_c with the critical temperature T_c given by

$$T_c = \bar{T}_c(2U_{\text{ab}} - U_{\text{aa}} - U_{\text{bb}})/4k_B. \quad (7)$$

with the Boltzmann constant k_B and the dimensionless coefficient $\bar{T}_c \approx 2.27$ for the square lattice. For $T < T_c$, the binary mixture phase separates into a cholesterol-poor phase β and a cholesterol-rich phase α . The corresponding coexistence region has the midline $X_{\text{ml}} = \frac{1}{2}$ and the width $\Delta X = [1 - (\sinh(zT_c/T))^{-4}]^{1/8}$ with $z = 2/\bar{T}_c \approx 0.88$, see ref. 14.

If all interaction energies U_{ij} are reduced by the same factor, $\zeta_\Sigma < 1$, the critical temperature T_c attains the reduced value $T_c(\Sigma) = \zeta_\Sigma T_c(0)$ as follows from (7). Applying this reduction factor to the critical temperature $T_c = 48$ °C = 321 K as shown in Fig. 2, we obtain the reduced critical temperatures $T_c = 320.5$ K = 47.5 °C for $\Sigma = 0.1$ mN m^{-1} and $T_c = 316$ K = 43 °C for $\Sigma = 1$ mN m^{-1} . We thus conclude that a tension of 0.1 mN m^{-1} should have essentially no effect on the phase diagram in Fig. 2 whereas a tension of 1 mN m^{-1} may lead to a substantial reduction of the coexistence region.

A reduction of the critical temperature is also obtained if the tension primarily reduces the interactions $|U_{\text{aa}}|$ and $|U_{\text{bb}}|$ between two identical molecules but leaves the cholesterol-phospholipid interactions U_{ab} essentially unchanged. On the other hand, the relation (7) implies that the critical temperature can also be increased by tension. Indeed, a tension-induced increase of T_c is obtained if the tension primarily reduces the interaction energy $|U_{\text{ab}}|$ between the cholesterol and phospholipid molecules.

So far, the tension-dependence of the phase behavior has not been addressed experimentally for the binary mixtures considered here. On the other hand, such experiments have been performed for three-component membranes consisting of cholesterol and two different lipids.^{21–23} In two of these studies, the tendency for domain formation was found to be increased by tension^{21,22} whereas the opposite behavior was found in ref 23. In the latter study, a membrane of fixed composition was studied and the temperature was decreased down to the

miscibility temperature, at which the membrane phase separated into large domains. An increase of membrane tension by 0.1 mN m^{-1} was found to decrease the miscibility temperature by a few tenths of a degree Kelvin. This reduction is rather consistent with the theoretical estimate obtained above for the same tension. Therefore, as long as the membrane tension is small compared to 1 mN m^{-1} , we can ignore the effects of membrane tension on the phase diagram in Fig. 2.

In the following, we will focus on such tensions in order to disentangle the effects of distinct membrane environments from those induced by membrane tension. Note that such a restriction on membrane tension also implies a restriction on the spontaneous membrane curvature, which leads to a spontaneous tension.²⁸ Thus, the spontaneous curvature should be small compared to $1/20 \text{ nm}$ in order to have a negligible influence on the phase diagram. In practice, these restrictions on the tension and spontaneous curvature do not provide strong limitations because the tension should always be small compared to the tension of rupture, which is of the order of a few mN m^{-1} .

3 Theoretical description of free membranes

For a statistical-mechanical description of the free membranes, we need to specify the basic control parameters for these membranes. In principle, we can control the molecular numbers \mathcal{N}_a and \mathcal{N}_b , the membrane tension Σ , as well as the temperature T . In practice, the tension can depend on a variety of constraints and forces and its precise value is often difficult to determine experimentally. It is therefore convenient to replace the tension by the membrane area $\mathcal{A} = \mathcal{A}(T, \Sigma, \mathcal{N}_a, \mathcal{N}_b)$ which can be directly measured for many membrane systems. Thus, we will consider the molecular numbers \mathcal{N}_a and \mathcal{N}_b , the membrane area \mathcal{A} , as well as the temperature T as the basic control parameters. These control parameters correspond to the canonical ensemble with the free energy $\mathcal{F} = \mathcal{F}(T, \mathcal{A}, \mathcal{N}_a, \mathcal{N}_b)$. Note that membrane tension Σ and membrane area \mathcal{A} play the same role as pressure and volume for bulk liquids and are, thus, related by a Legendre transformation as in bulk thermodynamics.

Any statistical-mechanical description of the free membrane now starts with the configuration energy $\mathcal{E}\{\text{conf}\}$, which determines the free energy *via*

$$\mathcal{F} = -k_B T \ln \left(\sum_{\text{conf}} \exp[-\mathcal{E}\{\text{conf}\}/k_B T] \right) \quad (8)$$

where the summation runs over all configurations of the N_a and N_b molecules within the free membrane. In principle, the configuration energy $\mathcal{E}\{\text{conf}\}$ contains many different interaction terms between the lipid and cholesterol molecules. In practice, we can determine many aspects of the phase behavior without specifying the form of these interactions.

3.1 Chemical potentials

The chemical potentials of the two molecular species are given by

$$\mu_a = \left(\frac{\partial \mathcal{F}}{\partial \mathcal{N}_a} \right)_{T, \mathcal{A}, \mathcal{N}_b} \quad \text{and} \quad \mu_b = \left(\frac{\partial \mathcal{F}}{\partial \mathcal{N}_b} \right)_{T, \mathcal{A}, \mathcal{N}_a}. \quad (9)$$

Because the chemical potentials μ_a and μ_b are intensive variables (in the sense of thermodynamics), they can only depend on other intensive variables, provided here by temperature T , tension Σ , and mole fraction X . Because we will focus on tensions $\Sigma \leq 0.1 \text{ mN m}^{-1}$, for which we can ignore tension-induced changes of the phase diagram, we will also ignore the tension-dependence of the chemical potentials.

The dependence of the chemical potentials on the mole fraction X will be expressed in the form

$$\mu_a = G_a(X) \quad \text{and} \quad \mu_b = G_b(X) \quad (10)$$

where the temperature-dependence of the functions $G_a(X)$ and $G_b(X)$ has been suppressed for notational simplicity. These two functions have some useful properties that follow from thermodynamic stability. Indeed, if two membrane segments are allowed to exchange molecules, they approach a state of chemical equilibrium, in which both segments have the same chemical potential. Furthermore, if the two segments initially differ in their chemical potentials, the equilibrium state is approached *via* an overall flux of molecules from the segment with the higher chemical potential to the segment with the lower one. Thermodynamic stability of the equilibrium state then implies that the derivative of the chemical potential with respect to molecular number must not be negative. Therefore, the functions $G_a(X_a)$ and $G_b(X_a)$ satisfy

$$\frac{\partial \mu_a}{\partial X} = \frac{\partial G_a(X)}{\partial X} \geq 0. \quad (11)$$

and

$$\frac{\partial \mu_b}{\partial X} = \frac{\partial G_b(X)}{\partial X} = -\frac{\partial \mu_b}{\partial X_b} \leq 0 \quad (12)$$

where $X_b = 1 - X$ has been used. In both relations (11) and (12), the equality signs correspond to a coexistence region between an a-rich and an a-poor phase.

3.2 Molecular areas of membrane components

For fixed values of the control parameters $T, \mathcal{A}, \mathcal{N}_a$, and \mathcal{N}_b , the a- and b-molecules have certain molecular areas, A_a and A_b . These areas can be defined in a variety of ways and these definitions have been applied both to molecular dynamics simulations²⁹⁻³¹ and to scattering experiments.^{32,33} An early simulation study of cholesterol-DPPC membranes²⁹ at $50 \text{ }^\circ\text{C}$ used a volumetric definition and concluded that both the molecular area A_a of cholesterol and the area A_b of DPPC were essentially constant for all mole fractions X within the range $0.05 \leq X \leq 0.4$.

An alternative, thermodynamic definition is provided by the specific molecular areas as introduced in ref. 30 and applied in the analysis of both X-ray³² and neutron³³ scattering data. The specific molecular area of cholesterol was found to change substantially with cholesterol's mole fraction X for

cholesterol–DMPC and cholesterol–DOPC at 30–33 °C, see ref. 32, but to remain essentially constant for binary mixtures of cholesterol and monounsaturated diacylphosphatidylcholines at 30 °C, see ref. 33.

As far as we know, the molecular areas of cholesterol–DPPC membranes have not been studied experimentally, so far, for the compositions and temperatures, for which fluid–fluid coexistence has been proposed, see Fig. 2. Thus, we will ignore a possible composition-dependence of the molecular areas and assume that they attain, at fixed temperature, a constant value within the composition range depicted in Fig. 2. Furthermore, we will also assume that the molecular areas of A_a and A_b are positive, as found in the simulation study of cholesterol–DPPC membranes at 50 °C.²⁹

3.3 Relative chemical potential

Because the a- and b-molecules are densely packed to form a bilayer of total surface area $2\mathcal{A}$, the numbers \mathcal{N}_a and \mathcal{N}_b of the two molecular species are not independent but are related *via*

$$\mathcal{N}_a A_a + \mathcal{N}_b A_b = 2\mathcal{A}. \quad (13)$$

We now imagine to couple the membrane to two reservoirs for a- and b-molecules with two chemical potentials, μ_a and μ_b . Because of the constraint (13), we have to exchange molecules with both reservoirs simultaneously. Indeed, if we want to move m molecules from the a-reservoir into the membrane, we have to move $n = mA_a/A_b$ from the membrane into the b-reservoir. The corresponding change in free energy of the membrane is given by $m\mu_a - n\mu_b$, which is equal to $m\Delta\mu$ if we define the relative chemical potential

$$\Delta\mu \equiv A_a \left[\frac{\mu_a}{A_a} - \frac{\mu_b}{A_b} \right]. \quad (14)$$

Using the functions $G_a(X)$ and $G_b(X)$ as introduced in (10), the relative chemical potential becomes

$$\Delta\mu = A_a \left[\frac{G_a(X)}{A_a} - \frac{G_b(X)}{A_b} \right] \equiv G(X) \quad (15)$$

where we again suppress the temperature-dependence of $G(X)$ for notational simplicity. If the molecular areas A_a and A_b of the two molecular species are equal, the expression (14) for the relative chemical potential simplifies and becomes

$$\Delta\mu = \mu_a - \mu_b = G_a(X) - G_b(X) \quad (A_a = A_b) \quad (16)$$

as in the lattice binary mixture.¹⁴

Using the stability relations (11) and (12) together with the definition (14) of the relative chemical potential $\Delta\mu$, we conclude that this chemical potential must also be a non-decreasing function of X , *i.e.*,

$$\Delta\mu = G(X) \text{ with } \partial G/\partial X \geq 0, \quad (17)$$

where the equality sign applies to the X -values within the coexistence region as given by (2), see next subsection.

3.4 Phase diagram: semigrand canonical ensemble

The phase diagram displayed in Fig. 2 corresponds to the canonical ensemble, in which we control the molecular number \mathcal{N}_a and \mathcal{N}_b of the two molecular species, the typical situation in experimental studies. From a theoretical point of view, it is also useful to consider the grand canonical ensemble, in which we control the chemical potentials rather than the molecular numbers. More precisely, because of the condition (13), the appropriate statistical ensemble is provided by a semigrand canonical ensemble, in which we control the relative chemical potential $\Delta\mu$ as given by (14). Such ensembles have also been used in the context of bulk liquids.^{34–36}

The grand canonical description is obtained if we replace the Boltzmann factor $\exp[-(\mathcal{E}\{\text{conf}\})/k_B T]$ in (8) by the statistical weight $\exp[-(\mathcal{E}\{\text{conf}\} - \mu_a \mathcal{N}_a - \mu_b \mathcal{N}_b)/k_B T]$. Furthermore, when \mathcal{N}_b is expressed in terms of \mathcal{N}_a *via* the relation (13), the statistical weight for the semigrand canonical ensemble assumes the form

$$\exp[-(\mathcal{E}\{\text{conf}\} - \Delta\mu \mathcal{N}_a)/k_B T] \quad (18)$$

with the relative chemical potential $\Delta\mu$ as in eqn (14).

Because both temperature and relative chemical potential are intensive variables, phase separation into the liquid-ordered and liquid-disordered phases α and β now occurs along the demixing curve

$$\Delta\mu = \mu_{\alpha\beta}(T) \text{ for } T_t < T \leq T_c \quad (19)$$

within the $(T, \Delta\mu)$ -plane. The demixing curve will, in general, also depend on the membrane tension but this dependence should be negligible for tensions $\Sigma \leq 0.1 \text{ mN m}^{-1}$ as considered here.

Inserting the relation $\Delta\mu = G(X)$ into the expression (19), we obtain

$$G(X) = \mu_{\alpha\beta}(T) \text{ for } X_\beta(T) < X \leq X_\alpha(T), \quad (20)$$

i.e., the function $G(X)$ attains the constant value $\mu_{\alpha\beta}(T)$ within the $\alpha\beta$ coexistence region.

4 Membranes exposed to two environments

4.1 Partitioning into two membrane segments

We now consider situations, in which the cholesterol–phospholipid membranes discussed in the previous section are exposed to two different environments. One example is provided by vesicle adhesion as depicted in Fig. 1. Other examples are solid-supported membranes that span holes or pores in the support as well as membranes that adhere to chemically patterned surfaces with two types of surface domains.¹⁴ In all of these cases, the two environments lead to two distinct membrane segments, $\mathcal{A}^{[1]}$ and $\mathcal{A}^{[2]}$.

For vesicle adhesion as in Fig. 1, the two membrane segments are provided by the unbound segment $\mathcal{A}^{[1]}$ and the bound segment $\mathcal{A}^{[2]}$. For partially supported membranes such

as hole- or pore-spanning membranes, the segment $\mathcal{S}^{[1]}$ spans the pores or holes, whereas the segment $\mathcal{S}^{[2]}$ is firmly attached to the underlying support. Likewise, a chemically patterned surface typically consists of two different types of surface domains. In this case, we take the membrane segments $\mathcal{S}^{[1]}$ to be located adjacent to the less adhesive surface domains.

Because the membrane consists of two segments, the total number \mathcal{N} of membrane molecules can be divided up as

$$\mathcal{N} = \mathcal{N}^{[1]} + \mathcal{N}^{[2]} + \mathcal{N}^{[1/2]} \quad (21)$$

where $\mathcal{N}^{[m]}$ is the overall number of molecules in segment $\mathcal{S}^{[m]}$ and $\mathcal{N}^{[1/2]}$ represents the overall number of molecules within the border region between these two segments. We will assume that the segments are large in the sense that

$$\mathcal{N}^{[m]} \gg \mathcal{N}^{[1/2]} \text{ for } m = 1, 2 \quad (22)$$

and will, thus, ignore contributions arising from the intermediate border region. For hole- and pore-spanning membranes, this condition will already be fulfilled for relatively small hole and pore diameters of the order of 100 nm. Likewise, the condition will be met for adhering vesicles with a linear size $\sqrt{\mathcal{A}/4\pi}$ that exceeds 10 μm , for which the ratio $\mathcal{N}^{[1/2]}/\mathcal{N}^{[m]} \leq 0.01$. For adhering vesicles with a smaller size, the relative importance of the border region can be determined by minimizing the bending energy of the vesicle membrane.^{18,19}

The configurational energy of an adhering membrane consisting of two membrane segments is then given by

$$\mathcal{E}\{\text{conf}\} \approx \mathcal{E}^{[1]}\{\text{conf}\} + \mathcal{E}^{[2]}\{\text{conf}\} \quad (23)$$

where $\mathcal{E}^{[m]}$ is the configurational energy of segment $\mathcal{S}^{[m]}$. Likewise, the total membrane area \mathcal{A} can then be decomposed as

$$\mathcal{A} \approx \mathcal{A}^{[1]} + \mathcal{A}^{[2]} \quad (24)$$

where $\mathcal{A}^{[m]}$ is the surface area of segment $\mathcal{S}^{[m]}$.

As we will see further below, the phase behavior of the segmented membrane depends only on one geometric parameter, the area fraction

$$q^{[1]} \equiv \frac{\mathcal{A}^{[1]}}{\mathcal{A}} = \frac{\mathcal{A}^{[1]}}{\mathcal{A}^{[1]} + \mathcal{A}^{[2]}}. \quad (25)$$

The parameter $q^{[1]}$ can vary within the range $\frac{1}{2} \leq q^{[1]} < 1$ for vesicle adhesion and within $0 \leq q^{[1]} < 1$ for partially supported membranes.

4.2 Adhesion-induced tension

The adhering membranes described in the previous subsection are subject to some tension.^{18,19} For a membrane of an adhering vesicle, this tension arises from the competition between the osmotic pressure difference across the unbound segment and the attraction towards the adhesive surface. For a hole- or pore-spanning membrane, the tension arises from the additional energy that the membrane could gain by moving onto the solid

support.¹⁹ Likewise, for a chemically patterned surface, the membrane could lower its energy by moving onto the more adhesive surface domains.

For vesicle adhesion as shown in Fig. 2, the adhesion-induced tension is of the order of the adhesion strength W , reflecting the balance between the attraction towards the adhesive surface and the osmotic pressure difference between the interior and exterior compartments of the vesicle.^{18,19} Experimentally, one can distinguish a weak adhesion regime with $|W| \leq 10^{-3} \text{ mN m}^{-1}$ from a strong adhesion regime with $|W| \geq 10^{-3} \text{ mN m}^{-1}$, see ref. 37. Here, we will focus on surfaces with an adhesion strength $|W| \leq 0.1 \text{ mN m}^{-1}$. As previously explained in Section 2.2, we can then ignore tension-induced changes of the phase diagram.

In general, the two membrane segments $\mathcal{S}^{[1]}$ and $\mathcal{S}^{[2]}$ can experience distinct tensions as observed, *e.g.*, for vesicle membranes enclosing two droplets that consist of two different aqueous phases.^{28,38} In the latter case, the different tensions arise from different spontaneous curvatures of the membrane segments. However, when these spontaneous curvatures can be ignored, the two segments experience the same tension, *i.e.*,

$$\Sigma^{[1]} = \Sigma^{[2]} \equiv \Sigma. \quad (26)$$

in mechanical equilibrium. This relation shows explicitly that the tension of fluid membranes plays the same role as the pressure of bulk liquids.

4.3 Molecular affinities within membrane segments

We will now use the free membrane described in the previous section as a reference system. This freely suspended and fully hydrated membrane is governed by the configuration energy $\mathcal{E}\{\text{conf}\}$, see (8) and (18). When exposed to an adhesive environment, the a- and b-molecules within the corresponding membrane segment experience additional interactions with this environment. We can then write the configuration energy $\mathcal{E}^{[m]}$ of segment $\mathcal{S}^{[m]}$ in the form

$$\mathcal{E}^{[m]}\{\text{conf}\} = \mathcal{E}\{\text{conf}\} + U_a^{[m]}\mathcal{N}_a + U_b^{[m]}\mathcal{N}_b \quad (27)$$

which defines the excess interaction energies or molecular affinities $U_a^{[m]}$ and $U_b^{[m]}$ acting on the a- and b-molecules within segment $\mathcal{S}^{[m]}$. By definition, the molecular affinities vanish for a free membrane.

We use the sign convention that attractive interactions between the molecules and the environments correspond to *negative* values of the excess interaction energies, *i.e.*,

$$U_a^{[m]} < 0 \text{ and } U_b^{[m]} < 0 \quad (28)$$

when the a- and b-molecules are attracted by the environment of segment $\mathcal{S}^{[m]}$.

In the following sections, the molecular affinities $U_a^{[m]}$ and $U_b^{[m]}$ are taken to be constant within each membrane segment $\mathcal{S}^{[m]}$. Thus, we assume that each environment has a uniform chemical composition. If an environment is provided by a solid or a solid-like substrate, the associated molecular affinities may

exhibit quenched local variations. The possible effects of such disordered environments onto the phase behavior are discussed in Section 8 below.

4.4 Chemical potentials of membrane segments

It follows from the expression (27) for the configuration energy of segment $\mathcal{S}^{[m]}$ that the segmental free energy $\mathcal{F}^{[m]}$ is given by

$$\mathcal{F}^{[m]} \approx \mathcal{F} + U_a^{[m]} \mathcal{N}_a + U_b^{[m]} \mathcal{N}_b \quad (29)$$

where the asymptotic equality reminds us that we consider large membrane segments and ignore correction terms arising from the finite size or the boundaries of these segments.

The chemical potential $\mu_a^{[m]} = \partial \mathcal{F}^{[m]} / \partial \mathcal{N}_a$ of the a-molecules within segment $\mathcal{S}^{[m]}$ is then given by

$$\mu_a^{[m]} = G_a(X^{[m]}) + U_a^{[m]} \quad (30)$$

with the function $G_a(X)$ as in (10). Likewise, the chemical potential of the b-molecules within this segment has the form

$$\mu_b^{[m]} = G_b(X^{[m]}) + U_b^{[m]} \quad (31)$$

with the function $G_b(X)$ as in (10).

4.5 Relative chemical potentials of membrane segments

Using the definition of the relative chemical potential in eqn (14) together with the expressions (30) and (31) for the two segmental chemical potentials, we obtain the relative chemical potential

$$\Delta\mu^{[m]} = G(X^{[m]}) + \Delta U^{[m]} \quad (32)$$

for membrane segment $\mathcal{S}^{[m]}$ with the function $G(X)$ as in (15) and the *relative affinity*

$$\Delta U^{[m]} \equiv A_a \left[\frac{U_a^{[m]}}{A_a} - \frac{U_b^{[m]}}{A_b} \right], \quad (33)$$

where A_a and A_b denote the molecular areas of the a- and b-molecules as before. For a free membrane segment $\mathcal{S}^{[m]}$, the molecular affinities $U_a^{[m]}$ and $U_b^{[m]}$ vanish by definition and the relative affinity $\Delta U^{[m]}$ vanishes as well.

In order to eliminate one molecular parameter, it is instructive to consider the special case with $A_a = A_b$. The expression (33) for the relative affinity then simplifies and becomes

$$\Delta U^{[m]} = U_a^{[m]} - U_b^{[m]} \text{ for } A_a = A_b, \quad (34)$$

as in the lattice binary mixture or the equivalent Ising model.¹⁴

4.6 Sign of relative affinities

Our sign convention (28) for the molecular affinities $U_a^{[m]}$ and $U_b^{[m]}$ implies that the relative affinity $\Delta U^{[m]}$ as given by (33) is *positive* and *negative* if the b-molecules and the a-molecules are more strongly attracted by the environment of segment $\mathcal{S}^{[m]}$, respectively. More precisely, the relative affinity

$$\Delta U^{[m]} < 0 \text{ if } \frac{U_a^{[m]}}{A_a} < \frac{U_b^{[m]}}{A_b}, \quad (35)$$

i.e., provided the energy density of the excess interactions for the a-molecules is more negative than the corresponding energy density for the b-molecules. A negative relative affinity $\Delta U^{[m]}$ implies an enrichment of the a-molecules and a depletion of the b-molecules in membrane segment $\mathcal{S}^{[m]}$ compared to a free segment. Likewise, a positive relative affinity $\Delta U^{[m]} > 0$ implies an enrichment of the b-molecules and a depletion of the a-molecules in $\mathcal{S}^{[m]}$ compared to a free membrane segment.

4.7 Phase transitions in membrane segments

Within the semigrand canonical ensemble, a free membrane segment undergoes phase separation along the demixing curve $\Delta\mu = G(X) = \mu_{\alpha\beta}(T)$ as described in Section 3.4 above. It then follows from the expression (32), that membrane segment $\mathcal{S}^{[m]}$ undergoes phase separation along the demixing curve

$$\Delta\mu^{[m]} = \mu_{\alpha\beta}(T) + \Delta U^{[m]} \equiv \mu_{\alpha\beta}^{[m]}(T) \text{ for } T_t < T \leq T_c. \quad (36)$$

As long as the relative affinities $\Delta U^{[1]}$ and $\Delta U^{[2]}$ of the two membrane segments are different, the demixing curves of the two segments are different as well and the two segments undergo two distinct phase transitions. Thus, the phase diagram in the $(\Delta\mu, T)$ -plane consists of two curves that are shifted against each other by the *affinity contrast*

$$\mu_{\alpha\beta}^{[2]} - \mu_{\alpha\beta}^{[1]} = \Delta U^{[2]} - \Delta U^{[1]} \equiv \Delta U \quad (37)$$

as shown schematically in Fig. 3. In this figure, the shape of the demixing lines $\Delta\mu^{[m]} = \mu_{\alpha\beta}^{[m]}(T)$ was chosen to resemble a typical vapor–liquid coexistence curve.^{39,40}

Therefore, a membrane consisting of two segments undergoes two phase transitions for any affinity contrast $\Delta U \neq 0$. If membrane segment $\mathcal{S}^{[1]}$ represents a free segment as for vesicle adhesion, see Fig. 1, the relative affinity $\Delta U^{[1]} = 0$, and the affinity contrast $\Delta U = \Delta U^{[2]}$. The same relation applies to hole- or pore-spanning membranes. For membranes supported

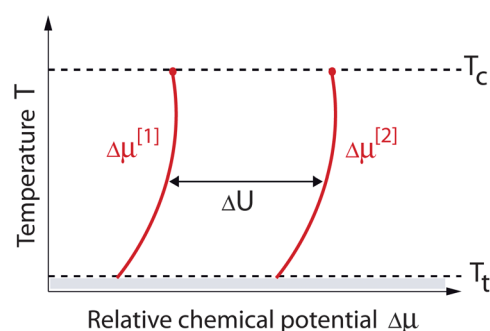


Fig. 3 Phase diagram for two membrane segments as a function of relative chemical potential $\Delta\mu$ and temperature T . Segment $\mathcal{S}^{[1]}$ undergoes phase separation along the demixing line $\Delta\mu = \Delta\mu^{[1]}(T)$ (red curve on the left), segment $\mathcal{S}^{[2]}$ along the demixing line $\Delta\mu = \Delta\mu^{[2]}(T)$ (red curve on the right) with $T_t < T \leq T_c$. The two demixing lines are separated by the affinity contrast ΔU and end in two critical points.

by a chemically patterned surface, on the other hand, no membrane segment represents a free segment and both $\Delta U^{[1]}$ and $\Delta U^{[2]}$ will be different from zero.

5 Composition of membrane segments

The chemical potentials discussed in the previous section are useful from a theoretical but not from an experimental point of view. In order to make predictions that can be scrutinized by experiments, we will now consider the mole fractions $X^{[1]}$ and $X^{[2]}$ within the two membrane segments. We will show that we can determine these mole fractions from two general relations that describe the chemical equilibrium and the molecular partitioning between the two segments.

5.1 Chemical equilibrium between membrane segments

Since the two membrane segments $\mathcal{S}^{[1]}$ and $\mathcal{S}^{[2]}$ can freely exchange a- and b-molecules by lateral diffusion, they will attain a state of chemical equilibrium, in which the relative chemical potential $\Delta\mu^{[1]}$ of segment $\mathcal{S}^{[1]}$ is equal to the relative chemical potential $\Delta\mu^{[2]}$ of segment $\mathcal{S}^{[2]}$. It then follows from (32) that this chemical equilibrium is described by

$$\Delta\mu^{[1]} = G(X^{[1]}) + \Delta U^{[1]} = \Delta\mu^{[2]} = G(X^{[2]}) + \Delta U^{[2]} \quad (38)$$

or

$$G(X^{[1]}) = G(X^{[2]}) + \Delta U \quad (39)$$

with the affinity contrast $\Delta U = \Delta U^{[2]} - \Delta U^{[1]}$ as introduced in eqn (37).

The chemical equilibrium condition as described by (38) or (39) provides a relation between the two mole fractions $X^{[1]}$ and $X^{[2]}$. For $\Delta U = 0$, the solution of eqn (39) is simply given by $X^{[1]} = X^{[2]} = X$. For $\Delta U \neq 0$, useful insight into the solution of eqn (38) can be obtained *via* a graphical solution as depicted in Fig. 4 for the positive affinity contrast.

5.2 Segment compositions for positive affinity contrast

In Fig. 4, the two functions $\Delta\mu^{[1]} = G(X^{[1]}) + \Delta U^{[1]}$ and $\Delta\mu^{[2]} = G(X^{[2]}) + \Delta U^{[2]}$ have been plotted using the same X -axis for the two mole fractions $X^{[1]}$ and $X^{[2]}$. Any solution to eqn (38) can now be obtained from the intersections of these two functions with a horizontal line corresponding to the constant value $\Delta\mu = \Delta\mu_0$.

Inspection of Fig. 4 shows that the two mole fractions $X^{[1]}$ and $X^{[2]}$ are different for all values of $\Delta\mu_0$. More precisely, we can distinguish five different regimes for the value of $\Delta\mu_0$:

(i) For $\Delta\mu_0 < \mu_{\alpha\beta} + \Delta U^{[1]}$, both mole fractions are smaller than X_β , *i.e.*, both membrane segments attain uniform β phases, albeit with different compositions;

(ii) For $\Delta\mu_0 = \mu_{\alpha\beta} + \Delta U^{[1]}$, membrane segment $\mathcal{S}^{[1]}$ undergoes phase separation while segment $\mathcal{S}^{[2]}$ stays in a uniform *spectator phase*, *i.e.*,

$$X^{[2]} = X_*^{[2]}(T) \text{ for } X_\beta(T) \leq X^{[1]} \leq X_\alpha(T). \quad (40)$$

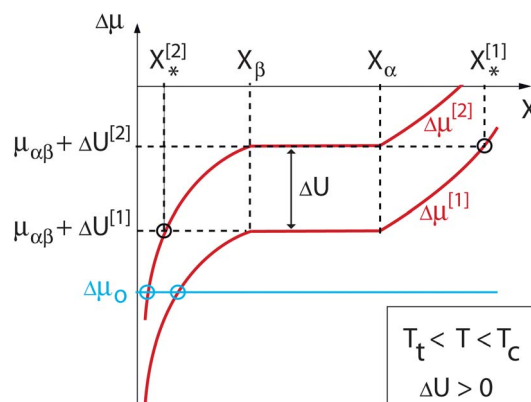


Fig. 4 Graphical solution of eqn (38) for temperature T within the range $T_t < T < T_c$ and positive affinity contrast ΔU . The variable X represents the two mole fractions, $X^{[1]}$ and $X^{[2]}$, the lower red curve corresponds to $\Delta\mu = \Delta\mu^{[1]}(X^{[1]})$, the upper one to $\Delta\mu = \Delta\mu^{[2]}(X^{[2]})$. All solutions for $X^{[1]}$ and $X^{[2]}$ can be obtained from the intersections of the two red curves with a horizontal line (light blue) corresponding to the constant value $\Delta\mu = \Delta\mu_0$ as explained in the text. The two mole fractions $X_*^{[1]}$ and $X_*^{[2]}$ correspond to uniform spectator phases in the membrane segments $\mathcal{S}^{[1]}$ and $\mathcal{S}^{[2]}$, respectively, see eqn (41) and (40).

(iii) For $\Delta\mu_0$ -values within the range $\mu_{\alpha\beta} + \Delta U^{[1]} < \Delta\mu_0 < \mu_{\alpha\beta} + \Delta U^{[2]}$, the mole fractions satisfy $X^{[1]} > X_\alpha$ and $X^{[2]} < X_\beta$, *i.e.*, the composition of segment $\mathcal{S}^{[1]}$ corresponds to a uniform α -phase whereas segment $\mathcal{S}^{[2]}$ has the composition of a uniform β -phase;

(iv) For $\Delta\mu_0 = \mu_{\alpha\beta} + \Delta U^{[2]}$, segment $\mathcal{S}^{[2]}$ undergoes phase separation while segment $\mathcal{S}^{[1]}$ now stays in a uniform spectator phase, *i.e.*,

$$X^{[1]} = X_*^{[1]} \text{ for } X_\beta \leq X^{[2]} \leq X_\alpha; \quad (41)$$

and

(v) Finally, for $\Delta\mu_0 > \mu_{\alpha\beta} + \Delta U^{[2]}$, both mole fractions exceed X_α , *i.e.*, both membrane segments attain uniform α -phases, again with different compositions.

Note that the choice of origin for the relative chemical potentials has no effect on the values of the two mole fractions $X^{[1]}$ and $X^{[2]}$. Indeed, we can shift all relative chemical potentials by an arbitrary constant without changing the values of these mole fractions as one can conclude from Fig. 4.

5.3 Negative affinity contrast and symmetry relations

The graphical solution displayed in Fig. 4 and the corresponding discussion in the previous subsection apply to *positive* values of the affinity contrast. For *negative* values of the affinity contrast, the curve $\Delta\mu^{[2]} = G(X^{[2]}) + \Delta U^{[2]}$ is located below the curve $\Delta\mu^{[1]} = G(X^{[1]}) + \Delta U^{[1]}$. Now, if we consider a certain affinity contrast $\Delta U < 0$ and shift the origin of the chemical potentials downward by $|\Delta U|$, we arrive at the same diagram as in Fig. 4 but with the segment indices [1] and [2] interchanged. Because the choice of origin for the relative chemical potentials does not affect the composition of two membrane segments, changing the sign of the affinity contrast ΔU is equivalent to interchanging the two membrane segments.

In particular, the mole fractions $X_*^{[2]}$ and $X_*^{[1]}$ of the two spectator phases satisfy the symmetry relation

$$X_*^{[2]}(T, -\Delta U) = X_*^{[1]}(T, +\Delta U), \quad (42)$$

which is equivalent to

$$X_*^{[1]}(T, -\Delta U) = X_*^{[2]}(T, +\Delta U), \quad (43)$$

for all values of T and ΔU , irrespective of the functional form of $G(X)$.

So far, we have discussed the consequences of the chemical equilibrium condition (38), which provides one relation between the two mole fractions $X^{[1]}$ and $X^{[2]}$. In order to uniquely determine these variables, we need a second relation between them. This second relation is provided by the partitioning of the molecules between the two membrane segments as discussed next.

5.4 Partitioning of membrane molecules

Because the total number of molecules is conserved within the membrane, the mole fractions $X^{[1]}$ and $X^{[2]}$ satisfy the relation

$$\frac{\mathcal{N}^{[1]}}{\mathcal{N}} X^{[1]} + \left(1 - \frac{\mathcal{N}^{[1]}}{\mathcal{N}}\right) X^{[2]} = X \quad (44)$$

where $\mathcal{N}^{[1]}$ is the combined number of a- and b-molecules within membrane segment $\mathcal{S}^{[1]}$ and \mathcal{N} is the total number of molecules within both segments.

The number fraction $\mathcal{N}^{[1]}/\mathcal{N}$ can be expressed in terms of the overall area fraction $q^{[1]} = \mathcal{A}^{[1]}/\mathcal{A}$. Using the relations $\mathcal{N}^{[1]} = \mathcal{N}_a^{[1]} + \mathcal{N}_b^{[1]}$ and $2\mathcal{A}^{[1]} = A_a \mathcal{N}_a^{[1]} + A_b \mathcal{N}_b^{[1]}$ as well as the corresponding relations for $\mathcal{N}^{[2]}$ and $\mathcal{A}^{[2]}$, one finds after some algebra that the relation (44) is equivalent to

$$q^{[1]}f(X^{[1]}) + (1 - q^{[1]})f(X^{[2]}) = f(X) \quad (45)$$

with the function

$$f(X) \equiv \frac{A_a X}{A_a X + A_b(1 - X)}. \quad (46)$$

For each membrane segment, the quantity $Y = f(X)$ represents the fraction of the segment's total surface area that is occupied by a-molecules. If the a- and b-molecules have the same molecular area, one has $f(Y) = Y$ and the relation (45) attains the linear form

$$q^{[1]}X^{[1]} + (1 - q^{[1]})X^{[2]} = X \text{ for } A_a = A_b. \quad (47)$$

The partitioning of the membrane molecules as described by (45) or (47) provides the second relation between the molar fractions $X^{[1]}$ and $X^{[2]}$ of the a-molecules within the two membrane segments.

The general partitioning relation (45) depends on the area fraction $q^{[1]}$ of the segment $\mathcal{S}^{[1]}$ and on the ratio A_b/A_a of the two molecular areas. Because the latter parameter is not known for the relevant composition and temperature range in Fig. 2, we will eliminate this parameter in the following and use the linear

partitioning relation (47). It is straightforward, however, to extend our computation to any value $A_b/A_a \neq 1$.

6 Coexistence regions for membrane segments

Using a combination of the chemical equilibrium relation (39) and the partitioning relation (47), the phase behavior of the segmented membranes can now be obtained as a function of membrane composition X and temperature T . For free membranes, the corresponding phase diagram in the (X, T) -plane exhibits one coexistence region between a liquid-disordered phase β and a liquid-ordered phase α , see Fig. 2. For membranes exposed to two different environments as considered here, the phase diagram within the (X, T) -plane now contains two coexistence regions, one such region for each membrane segment. Several such phase diagrams are displayed in Fig. 5 and 6 for positive and negative values of the affinity contrast, respectively.

As previously mentioned, positive affinity contrasts apply to adhesive surfaces (or environments) that attract the phospholipid or b molecules more strongly than the cholesterol or a molecules. In the opposite case, the affinity contrast is negative.

In order to simplify the terminology of the following discussion, we will now use the language of vesicle adhesion and refer to the two membrane segments $\mathcal{S}^{[1]}$ and $\mathcal{S}^{[2]}$ as the unbound and bound segments, respectively. Furthermore, we will use the expression '(un)bound coexistence region' as an abbreviation for 'coexistence region of (un)bound membrane segment'. In both Fig. 5 and 6, the bound and unbound coexistence regions are displayed in red and blue, respectively. Comparison between the two figures shows that the two coexistence regions interchange their relative positions if one changes the sign of the affinity contrast.

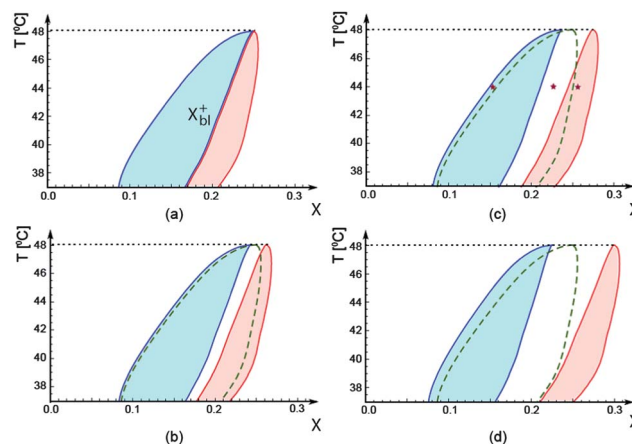


Fig. 5 Phase diagrams for the same binary mixture as in Fig. 2 but for vesicle membranes exposed to an adhesive surface with a positive affinity contrast $\Delta U > 0$. The four diagrams correspond to different values of the reduced contrast $\Delta u = \Delta U/(k_B T)$ for fixed area fraction $q^{[1]} = 2/3$: (a) $\Delta u = 0^+$, (b) $\Delta u = 0.1$, (c) $\Delta u = 0.2$, and (d) $\Delta u = 0.4$. The blue and red regions represent the two-phase coexistence regions of the unbound and bound membrane segments, respectively. The coexistence region of the free vesicle membrane (broken line) is included for comparison. All critical points are located at the same critical temperature T_c (horizontal dotted lines), the boundary line X_{bl}^+ in (a) is given by eqn (61) below, the three purple stars in (c) correspond to the three domain patterns as shown in the right column of Fig. 1.

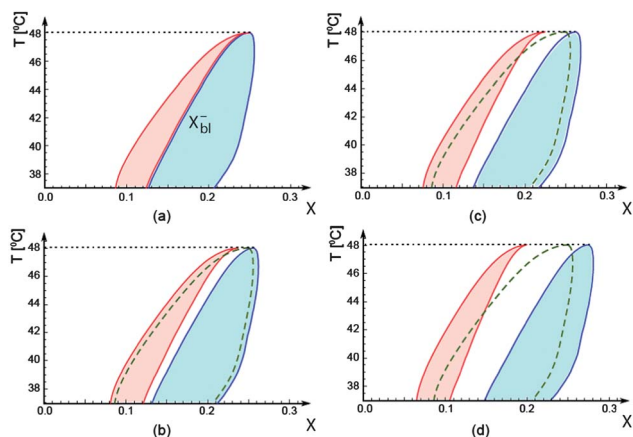


Fig. 6 Phase diagrams for the same binary mixture as in Fig. 2 but for vesicle membranes exposed to an adhesive surface with a *negative* affinity contrast $\Delta U < 0$. The four diagrams correspond to different values of the reduced contrast $\Delta u = \Delta U/(k_B T)$ for fixed area fraction $q^{[1]} = 2/3$: (a) $\Delta u = 0^-$, (b) $\Delta u = -0.1$, (c) $\Delta u = -0.2$, and (d) $\Delta u = -0.4$. The red and blue regions represent again the two-phase coexistence regions of the bound and unbound membrane segments but, compared to Fig. 5, these two regions have now swapped their relative positions. The coexistence region of the free vesicle membrane (broken line) is included for comparison. The boundary line X_{bi}^- in (a) is given by eqn (63) below.

The domain patterns for the adhering vesicles as shown in the right column of Fig. 1 for a positive affinity contrast correspond to three concentration regimes as indicated by the three purple stars in Fig. 5(c). In general, we can distinguish five different composition regimes for fixed values of the area fraction $q^{[1]}$, affinity contrast ΔU , and temperature T within the interval $T_t < T < T_c$. For sufficiently small values of X , both membrane segments attain uniform β phases that differ in their composition. For sufficiently large values of X , both segments attain uniform α phases, again with different compositions. In between, we find the two coexistence regions of the two membrane segments, separated by an intermediate composition regime.

6.1 Coexistence regions of the unbound membrane segment

Phase separation and domain formation occurs exclusively in the *unbound* membrane segment for all mole fractions X that satisfy

$$X_{\beta}^{[1]}(T) < X < X_{\alpha}^{[1]}(T) \text{ for } T_t < T < T_c \quad (48)$$

with the β -binodal

$$X_{\beta}^{[1]} \equiv q^{[1]}X_{\beta}(T) + (1 - q^{[1]})X_{*}^{[2]}(T, \Delta U) \quad (49)$$

and the α -binodal

$$X_{\alpha}^{[1]} \equiv q^{[1]}X_{\alpha}(T) + (1 - q^{[1]})X_{*}^{[2]}(T, \Delta U), \quad (50)$$

corresponding to the blue coexistence regions in both Fig. 5 and 6. The width $\Delta X^{[1]} \equiv X_{\alpha}^{[1]} - X_{\beta}^{[1]}$ of these coexistence regions is given by the simple expression

$$\Delta X^{[1]} = q^{[1]}[X_{\alpha}(T) - X_{\beta}(T)] = q^{[1]}\Delta X(T), \quad (51)$$

where $\Delta X(T)$ represents the width of the coexistence region for the free membrane.

The expressions (49) and (50) for the two binodals of the unbound membrane segment depend on the composition $X_{*}^{[2]}$ of the bound spectator phase. This composition can be calculated explicitly as a power series in ΔU , see the ESI.† To leading order, one then finds

$$X_{*}^{[2]} \approx X_{\beta} - c_{\beta}X_{\beta}(1 - X_{\beta})\Delta U/(k_B T) \text{ for small } \Delta U > 0 \quad (52)$$

and

$$X_{*}^{[2]} \approx X_{\alpha} + c_{\alpha}X_{\alpha}(1 - X_{\alpha})\Delta U/(k_B T) \text{ for small } \Delta U < 0 \quad (53)$$

with dimensionless coefficients c_{α} and c_{β} of order one. These coefficients appear in the thermodynamic derivatives $(\partial\mu_{\alpha}/\partial X)_{x_{\beta}}$ and $(\partial\mu_{\alpha}/\partial X)_{x_{\beta}}$.† The phase diagrams in Fig. 5 and 6 have been computed with $c_{\alpha} = c_{\beta} = 1$.

6.2 Coexistence regions of the bound membrane segment

Likewise, phase domains will exclusively form in the *bound* membrane segments for all mole fractions within the range

$$X_{\beta}^{[2]}(T) < X < X_{\alpha}^{[2]}(T) \text{ for } T_t < T < T_c \quad (54)$$

with the β -binodal

$$X_{\beta}^{[2]} \equiv q^{[1]}X_{*}^{[1]}(T, \Delta U) + (1 - q^{[1]})X_{\beta}(T) \quad (55)$$

and the α -binodal

$$X_{\alpha}^{[2]} \equiv q^{[1]}X_{*}^{[1]}(T, \Delta U) + (1 - q^{[1]})X_{\alpha}(T), \quad (56)$$

corresponding to the red coexistence regions in both Fig. 5 and 6. The width $\Delta X^{[2]} = X_{\alpha}^{[2]} - X_{\beta}^{[2]}$ of the bound coexistence region is given by

$$\Delta X^{[2]} = (1 - q^{[1]})\Delta X(T) \equiv q^{[2]}\Delta X(T), \quad (57)$$

with $q^{[2]} = \mathcal{A}^{[2]}/\mathcal{A}$ and the width ΔX of the free coexistence region.

The expressions (55) and (56) for the two binodals of the bound membrane segment depend on the composition $X_{*}^{[1]}$ of the unbound spectator phase which behaves as

$$X_{*}^{[1]} \approx X_{\alpha} + c_{\alpha}X_{\alpha}(1 - X_{\alpha})\Delta U/(k_B T) \text{ for small } \Delta U > 0 \quad (58)$$

and

$$X_{*}^{[1]} \approx X_{\beta} - c_{\beta}X_{\beta}(1 - X_{\beta})\Delta U/(k_B T) \text{ for small } \Delta U < 0 \quad (59)$$

with the same dimensionless coefficients c_{α} and c_{β} as in eqn (52) and (53).†

6.3 Intermediate composition regime without domains

For any non-zero value of the affinity contrast ΔU , the two coexistence regions are separated by an intermediate composition regime *without any domain formation* even though the free membranes phase separate in this regime.

For *positive* values of ΔU as shown in Fig. 5, this intermediate composition regime is given by the mole fraction range

$$X_{\alpha}^{[1]}(T) \leq X \leq X_{\beta}^{[2]}(T) \quad (\Delta U > 0) \quad (60)$$

In the limit of small $\Delta U > 0$, the width of this intermediate regime vanishes and the two binodals $X_{\alpha}^{[1]}$ and $X_{\beta}^{[2]}$ merge into the boundary line

$$X_{bi}^{+}(T) = X_{\beta}(T) + q^{[1]}\Delta X(T) \quad (\Delta U = 0^{+}) \quad (61)$$

as depicted in Fig. 5(a).

For *negative* values of ΔU as displayed in Fig. 6, we again find five different composition regimes including an intermediate composition regime between the two coexistence regions as given by

$$X_{\alpha}^{[2]}(T) \leq X \leq X_{\beta}^{[1]}(T) \quad (\Delta U < 0) \quad (62)$$

In the limit of small $\Delta U < 0$, the width of this intermediate regime vanishes and the two binodals $X_{\alpha}^{[2]}$ and $X_{\beta}^{[1]}$ merge into the boundary line

$$X_{bi}^{-}(T) = X_{\alpha}(T) - q^{[1]}\Delta X(T) \quad (\Delta U = 0^{-}) \quad (63)$$

as shown in Fig. 6(a).

Thus, whereas the intermediate composition regime becomes difficult to detect for small values of the affinity contrast ΔU , the two coexistence regions for the bound and the unbound segments remain distinct for any nonzero affinity contrast. Therefore, intramembrane domains form either in the bound or in the unbound segment but never in both segments simultaneously for *arbitrarily small affinity contrasts* $\Delta U \neq 0$.

6.4 Small affinity contrasts as singular perturbations

The phase diagrams for small positive and small negative affinity contrasts as displayed in Fig. 5(a) and 6(a), reveal that small affinity contrasts represent singular perturbations. Indeed, for small positive affinity contrasts, the blue coexistence region in the (X, T) -plane is located to the left of the red coexistence region whereas these two regions swap their relative positions for small negative affinity contrasts. Likewise, the two boundary lines $X_{bi}^{-}(T)$ and $X_{bi}^{+}(T)$ as given by eqn (61) and (63) are different unless $q^{[1]} = \frac{1}{2}$. For $\Delta U = 0$, on the other hand, both segments have the same composition and we recover the single coexistence region of the free membrane without any boundary line. Therefore, if one considers the phase diagram in the $(\Delta U, X)$ -plane for fixed values of temperature T and area fraction $q^{[1]}$, the coexistence regions change discontinuously across the line $\Delta U = 0$ as shown in Fig. 7.

The singular behavior just described has its origin in the ΔU -dependence of the mole fractions $X_{*}^{[1]}$ and $X_{*}^{[2]}$ of the spectator phases. Indeed, comparison of eqn (58) and (59) shows that the fraction $X_{*}^{[1]}$ of the unbound spectator phase jumps from $X_{*}^{[1]} \approx X_{\alpha}$ for $\Delta U = 0^{+}$ to $X_{*}^{[1]} \approx X_{\beta}$ for $\Delta U = 0^{-}$ as we change the affinity contrast from small positive to small negative values. At the same time, the mole fraction $X_{*}^{[2]}$ of the bound spectator phase

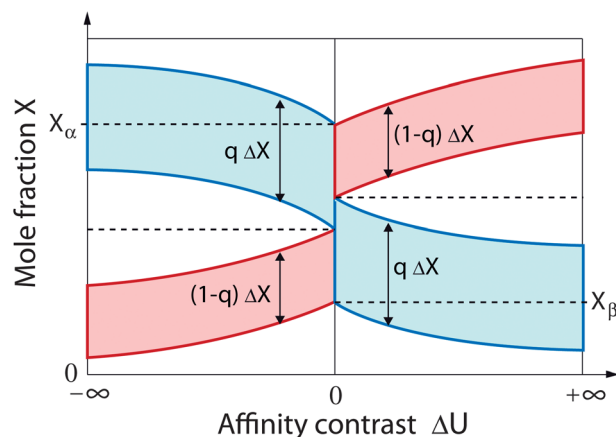


Fig. 7 Phase diagram as a function of the affinity contrast ΔU and mole fraction X for fixed values of temperature T and area fraction $q \equiv q^{[1]} > \frac{1}{2}$. The coexistence regions of the bound and unbound membrane segments are again colored in red and blue, respectively. The tie lines are now vertical. The blue coexistence region has the constant width $q\Delta X$, the width of the red region has the constant value $(1-q)\Delta X$. Note the discontinuous behavior of the binodals as one changes the affinity contrast ΔU from small positive to small negative values.

jumps from $X_{*}^{[2]} \approx X_{\beta}$ for $\Delta U = 0^{+}$ to $X_{*}^{[2]} \approx X_{\alpha}$ for $\Delta U = 0^{-}$ as follows from eqn (52) and (53). This discontinuous behavior of the composition of the spectator phases can also be directly deduced from the graphical construction in Fig. 4.

7 Membranes exposed to many environments

In the previous sections, we described the phase behavior of two-component membranes that are exposed to two different environments. In the present section, we generalize our results to two-component membranes exposed to M different environments and, thus, partitioned into M different membrane segments $\mathcal{A}^{[m]}$ with $m = 1, 2, \dots, M$. The total membrane area \mathcal{A} is now decomposed according to

$$\sum_{m=1}^M \mathcal{A}^{[m]} = \mathcal{A} \quad (64)$$

where $\mathcal{A}^{[m]}$ denotes the surface area of segment $\mathcal{A}^{[m]}$. The membrane segments are again taken to be large compared to the border regions between the segments. For giant vesicles with a linear size $\sqrt{\mathcal{A}/4\pi} = \rho \times 10 \mu\text{m}$, this condition is fulfilled for $M \leq \rho^2$. In adhering vesicles with a smaller size, the relative importance of the border regions can again be determined by minimizing the bending energy of the vesicle membrane.^{18,19}

The M segments are characterized by M relative affinities $\Delta U^{[m]}$ that are pair-wise distinct. If two segments, m and m' , had the same relative affinities $\Delta U^{[m]} = \Delta U^{[m']}$, we would combine them into one segment and decrease the total number M of different segments by one. We can then choose the index m in such a way that the relative affinities are ordered according to

$$\Delta U^{[1]} < \Delta U^{[2]} < \dots < \Delta U^{[M]}, \quad (65)$$

which leads to $M - 1$ affinity contrasts

$$\Delta U_m \equiv \Delta U^{[m+1]} - \Delta U^{[m]} \text{ for } m = 1, 2, \dots, M - 1. \quad (66)$$

The partitioning of the membrane molecules between the M membrane segments is now described by

$$\sum_{m=1}^M q^{[m]} X^{[m]} = X \text{ with } q^{[m]} \equiv \mathcal{A}^{[m]} / \mathcal{A}. \quad (67)$$

Generalizing the arguments in Section 6 to M membranes, see Fig. S1 and S2,[†] we find that the coexistence region of the free membrane is now divided into M distinct coexistence regions for the M segments. Therefore, *phase separation and domain formation is always confined to a single membrane segment*, while the other segments attain uniform spectator phases. Furthermore, the coexistence region for segment $\mathcal{A}^{[m]}$ has the width

$$\Delta X^{[m]}(T) = q^{[m]} \Delta X(T) \quad (68)$$

with the width ΔX of the free coexistence region. Thus, we now have the ‘sum rule’

$$\sum_{m=1}^M \Delta X^{[m]}(T) = \Delta X(T) = X_\alpha(T) - X_\beta(T), \quad (69)$$

i.e., the area of the coexistence region in the (X, T) -plane is conserved under the partitioning into the M segmental coexistence regions.

In the limit of small positive affinity contrasts $\Delta U_m = 0^+$, the coexistence region of the free membrane is divided by $M - 1$ boundary lines that have the form

$$X_{\text{bl},m}^+ = X_\beta(T) + [X_\alpha(T) - X_\beta(T)] \sum_{n=1}^m q^{[n]} \quad (70)$$

with $m = 1, 2, \dots, M - 1$. For $M = 2$, these equations reduce to eqn (61) for the boundary line X_{bl}^+ . As we increase the affinity contrast ΔU_m towards larger positive values, each boundary line $X = X_{\text{bl},m}^+$ opens up into an intermediate composition regime, in which all segments attain uniform phases without any domain formation.

In the limit of small negative affinity contrasts $\Delta U_m = 0^-$, the coexistence region of the free membrane is divided by $M - 1$ boundary lines that have the form

$$X_{\text{bl},m}^- = X_\alpha(T) - [X_\alpha(T) - X_\beta(T)] \sum_{n=1}^m q^{[n]} \quad (71)$$

with $m = 1, 2, \dots, M - 1$. For $M = 2$, these equations reduce to the single eqn (63) for the boundary line X_{bl}^- . As we decrease the affinity contrast ΔU_m towards larger negative values, each boundary line $X = X_{\text{bl},m}^-$ opens up into an intermediate composition regime, in which all segments attain uniform phases without any domain formation.

8 Environments with quenched disorder

In the previous sections, the environments were taken to have a uniform chemical composition. Such an environment can be

realized, *e.g.*, by a uniform solid substrate or a supported lipid bilayer. If the solid substrate contains many defects or immobilized impurities, the molecular affinities $U_a^{[m]}$ and $U_b^{[m]}$ may exhibit local variations that are quenched and do not change on the experimentally relevant time scales.

In principle, the affinity variations can pin the domain boundaries of the intramembrane domains and, thus, can suppress the coarsening of these domains. The latter pinning is expected to happen for quenched impurities or defects with uncorrelated positions and relatively large affinity variations. These variations then act as random fields, which lead to stable microdomain patterns as recently studied by Monte Carlo simulations of two-component membranes with quenched protein obstacles.⁴¹ Therefore, when a vesicle adheres to such a solid substrate, compare Fig. 1, the phase separation in the bound membrane segment may remain incomplete because the domain boundaries are pinned by the local affinity variations.

It is important to note, however, that the domain boundary between two intramembrane domains has a certain intrinsic width, which is of the order of the correlation length ξ for composition fluctuations, see, *e.g.*, ref. 42. Therefore, such a domain boundary feels *effective* affinity variations or random fields that remain when the molecular interactions are averaged over spatial regions of linear size ξ . Close to a critical point, the correlation length ξ diverges and the line tension λ vanishes as $k_B T / \xi$. A rough estimate for λ can be obtained from experimental studies of domains in ternary lipid mixtures as studied in ref. 43–45. In the latter case, the line tension was found to vary between 10^{-12} and 10^{-14} N, which implies that the correlation length ξ varies between 2 and 200 nm at room temperature. When we spatially average the molecular interactions between a solid-like environment and the membrane segment $\mathcal{A}^{[m]}$ over such large values of ξ , the effective molecular affinities $U_a^{[m]}$ and $U_b^{[m]}$ may be essentially constant even though the solid-like environment exhibits quenched disorder on smaller scales.

A somewhat different geometry is provided by a meshwork of cytoskeletal filaments, which interact with the membrane. When these filaments provide a sufficient number of strong pinning sites for one of the membrane components, they act as corral-like barriers that impede the phase separation process and confine the domains to the mesh size,⁴⁶ which is typically of the order of 100 nm.

9 Summary and outlook

In this paper, we studied two-component cholesterol–phospholipid membranes exposed to adhesive surfaces or environments that could be provided by solid surfaces or other membranes. We started with the phase behavior of the freely suspended membranes as depicted in the left column of Fig. 1. One example for the corresponding phase diagram is provided by Fig. 2 for cholesterol–DPPC membranes. When we bring such a membrane into contact with an adhesive surface as in the right column of Fig. 1, the membrane is exposed to two different environments and partitioned into two segments. Apart from exceptional cases, the two environments differ in their relative affinities for the two membrane components and,

thus, lead to a nonzero affinity contrast, $\Delta U \neq 0$, between the two segments. This affinity contrast strongly affects the phase diagram because it leads to a partitioning of the coexistence region of the free membrane into two distinct coexistence regions for the two membrane segments, see the examples shown in Fig. 5 and 6 for positive and negative values of ΔU , respectively.

In Section 7, we generalized our results to two-component membranes exposed to M different environments. The coexistence region of the free membrane is then partitioned into M distinct coexistence regions for the M membrane segments.

The partitioning of the coexistence region of the free membrane into $M \geq 2$ such regions for the different membrane segments has two important consequences. First, the domain formation within the two-component membrane is always *spatially confined to a single segment* $\mathcal{S}^{[m]}$. Second, for each segment, domains form only for compositions within the interval $X_{\beta}^{[m]} < X < X_{\alpha}^{[m]}$ with the *reduced composition range* $\Delta X^{[m]} = X_{\alpha}^{[m]} - X_{\beta}^{[m]} = q^{[m]}[X_{\alpha} - X_{\beta}]$ as in eqn (51), (57) and (68).

The *confinement of domain formation to single segments* and the *reduction of the composition range for segmental domain formation* are two very general results of our study and apply to any two-component membrane that exhibits fluid–fluid coexistence. Indeed, these two features follow from thermodynamic stability alone, which implies that the relative chemical potentials have the functional form as shown in Fig. 4 and S2 in the ESI.†

The phase diagrams for the binary cholesterol–DPPC membranes displayed in Fig. 5 and 6, on the other hand, involve certain simplifying assumptions and are, thus, semi-quantitative in nature. The first assumption was that we focused on membrane tensions $\Sigma \leq 0.1 \text{ mN m}^{-1}$. As explained in Sections 2.2 and 4.2, the phase diagrams should then be essentially independent of tension. Larger tension values are expected to shift the coexistence regions up or down but these shifts should be easy to distinguish from the partitioning of the coexistence region as induced by different membrane environments.

The second simplifying assumption was that we took the molecular areas A_a and A_b of cholesterol and DPPC to be equal when we calculated the phase diagrams in Fig. 5 and 6. This latter assumption reflects our limited knowledge about these molecular areas. If we had some improved estimates of these areas for the temperature and composition range displayed in Fig. 2, we could easily calculate improved phase diagrams by using the partitioning relation (45) that applies to any values of A_a and A_b .

The third simplification that we made in order to calculate the phase diagrams in Fig. 5 and 6 was to set two dimensionless coefficients, c_{α} and c_{β} , equal to one. These coefficients appear in the thermodynamic derivatives $(\partial\mu_a/\partial X)_{x_{\alpha}}$ and $(\partial\mu_a/\partial X)_{x_{\beta}}$ and enter the expressions (52) and (53) for the composition $X_{*}^{[2]}$ of the bound spectator phase as well as the expressions (58) and (59) for the composition $X_{*}^{[1]}$ of the unbound spectator phase. In order to calculate the precise values of c_{α} and c_{β} , we would have to consider a more detailed statistical–mechanical description, for which we specify the molecular interactions within the membranes.

It is important to note, however, that the partitioning of the coexistence curves for small positive or small negative values of the affinity contrasts, as described by the boundary lines $X = X_{\text{bl}}^{+}(T)$ in Fig. 5(a) and $X = X_{\text{bl}}^{-}(T)$ in Fig. 6(a) for two membrane segments as well as by the explicit expressions (70) and (71) for M segments, do *not* depend on the coefficients c_{α} and c_{β} but follow again from the graphical constructions in Fig. 4 and S2† and, thus, from thermodynamic stability alone.

One interesting consequence of the phase diagrams in Fig. 5 and 6 is that the two-component membranes can undergo, for a fixed value of the mole fraction X , two subsequent phase transitions as we change the temperature. As an example, let us consider the phase diagram in Fig. 5(b) corresponding to the area fraction $q^{[1]} = 2/3$ and affinity contrast $\Delta U = 0.1k_{\text{B}}T$ and let us choose the membrane composition $X = 0.2$. At low temperatures, the adhering vesicle is then in the bound or red coexistence region, which implies that intramembrane domains can form only in the bound membrane segment. At somewhat higher temperatures, the adhering vesicle explores the intermediate one-phase region and the vesicle membrane does not form any domains. At still higher temperatures closer to the critical temperature $T = T_c$, the adhering vesicle is in the unbound or blue coexistence region and domains form only in the unbound segment.

Phase separation within the membrane segments typically starts by the nucleation of a few small domains as schematically depicted in Fig. 1. These domains will then grow and coalesce. For a planar membrane segment exposed to a uniform environment, the line tension of the domain boundaries leads to an equilibrium pattern with two large domains, one liquid-ordered α domain and one liquid-disordered β domain. As previously shown in a somewhat different context,⁴⁷ the final shape of these two domains depends on the border of the planar membrane segment. If this border is incompletely wetted by the two membrane phases α and β , the domain boundary between the α and β domains forms a finite contact angle with the segment border. For complete wetting or dewetting, on the other hand, one domain is completely detached from the segment border.

A curved membrane segment exposed to a uniform environment may exhibit an equilibrium state with more than two domains as shown for free vesicles that are somewhat deflated and can, thus, attain a nonspherical shape.¹⁷ These multi-domain patterns arise from the competition between the line tension of the domain boundaries and the different bending rigidities of the α and β domains. For an adhering vesicle, on the other hand, the membrane is always under some tension as explained in Section 4.2. In the presence of such a tension, the unbound membrane segment of an adhering vesicle prefers to attain the shape of a spherical cap. Indeed, even relatively small tensions of the order of $10^{-3} \text{ mJ m}^{-2}$ lead to spherical cap shapes as observed for vesicles in contact with aqueous two-phase systems.³⁸ Therefore, phase separation in the unbound segment of an adhering vesicle, see Fig. 1(a), is also expected to lead to two large membrane domains. As in the case of a planar membrane segment, the actual shape of the two domains depends on the wetting properties of the segment border corresponding to the contact line of the vesicle.

In principle, quenched disorder in solid-like environments could lead to the pinning of domain boundaries and, thus, to microdomain patterns in the adjacent membrane segment. However, as long as the line tension in the binary mixtures considered here is comparable to or smaller than 10^{-12} N, the domain boundaries have a relatively large width and pinning effects are expected to be relatively small, see Section 8.

Our theoretical predictions are accessible to experimental studies. The simplest system seems to be provided by small vesicles or liposomes of binary cholesterol-phospholipid mixtures. It has been shown that such vesicles can form adsorbed or supported layers at solid surfaces.^{48–50} Such layers should be accessible to calorimetric measurements and then reveal the presence of two rather than one phase transition as one varies the temperature for fixed composition. Sufficiently dense layers of vesicles may even be accessible to spectroscopic methods and could then be compared with spectroscopic data obtained from bulk samples of non-adhering vesicles. Another experimental approach is provided by cholesterol-phospholipid membranes that span many small pores in a planar substrate surface.⁵¹ In fact, our results apply equally well to membranes adhering at curved surfaces with many small pores as provided by porous silica beads. The latter systems have already been studied by deuterium NMR.⁵² Finally, it would also be highly valuable to construct fluorescence labels, by which one can visualize the domains in the optical microscope.

Using these experimental approaches, one should be able to scrutinize our theoretical predictions about the phase behavior of cholesterol-phospholipid membranes exposed to adhesive surfaces or environments. Any experimental evidence for the restriction of the domains to single membrane segments or for the adhesion-induced suppression of the domain formation would provide strong evidence that the domains within cholesterol-phospholipid membranes do indeed arise from phase separation.

Finally, let us mention two generalizations of the theory described here. First, one can include the bilayer structure of the lipid membranes, which becomes relevant if the two leaflets of the bilayer exhibit different lipid compositions. Such compositional differences may arise, *e.g.*, when the area difference between the two leaflets changes because of changes in the total mean curvature of a vesicle. Because cholesterol molecules undergo relatively fast flip-flops compared to phospholipids, the elastic strain associated with such a change in area difference will initially relax *via* the redistribution of cholesterol between the two leaflets. Second, one can generalize our theory to fluid–fluid coexistence in ternary lipid mixtures. Such a mixture involves two mole fractions, say X_a and X_c , that can be varied independently and, thus, two relative chemical potentials, $\Delta\mu_a$ and $\Delta\mu_c$. Each adhesive environment is now characterized by three molecular affinities or two relative affinities, which act to shift the two relative chemical potentials of the adjacent membrane segment. Two-phase coexistence in the different membrane segments is then described by parallel lines in the $(\Delta\mu_a, \Delta\mu_c)$ -space, where the separation of these lines is determined by the affinity contrasts arising from the different relative affinities. Thus, M different environments will again

lead to M distinct phase transitions but it is now more tedious to determine the molecular compositions within the different membrane segments.

Acknowledgements

This study was supported by the German Research Foundation (DFG) *via* the international graduate programme IRTG 1524.

References

- 1 E. J. Shimshick and H. M. McConnell, *Biochem. Biophys. Res. Commun.*, 1973, **53**, 446–451.
- 2 B. R. Lentz, D. A. Barrow and M. Hoehli, *Biochemistry*, 1980, **19**, 1943–1954.
- 3 D. J. Recktenwald and H. M. McConnell, *Biochemistry*, 1981, **20**, 4505–4510.
- 4 M. R. Vist, MSc thesis, University of Guelph, Guelph, Ontario, Canada, 1984.
- 5 M. R. Vist and J. H. Davis, *Biochemistry*, 1990, **29**, 451–464.
- 6 M. B. Sankaram and T. E. Thompson, *Biochemistry*, 1990, **29**, 10670–10675.
- 7 T. P. W. McMullen and R. N. McElhaney, *Biochim. Biophys. Acta*, 1995, **1234**, 90–98.
- 8 S. L. Veatch and S. L. Keller, *Biochim. Biophys. Acta*, 2005, **1746**, 172–185.
- 9 S. L. Veatch, O. Soubias, S. L. Keller and K. Gawrisch, *Proc. Natl. Acad. Sci. U. S. A.*, 2007, **104**, 17650–17655.
- 10 J. H. Davis, J. J. Clair and J. Juhasz, *Biophys. J.*, 2009, **96**, 521–539.
- 11 D. Marsh, *Biochim. Biophys. Acta*, 2010, **1798**, 688–699.
- 12 J. H. Ipsen, G. Karlström, O. G. Mouritsen, H. Wennerström and M. J. Zuckermann, *Biochim. Biophys. Acta*, 1987, **905**, 162–172.
- 13 H. M. McConnell and M. Vrljic, *Annu. Rev. Biophys. Biomol. Struct.*, 2003, **32**, 469–492.
- 14 T. Rouhiparkouhi, T. R. Weikl, D. E. Discher and R. Lipowsky, *Int. J. Mol. Sci.*, 2013, **14**, 2203–2229.
- 15 R. Lipowsky, *J. Phys. II*, 1992, **2**, 1825–1840.
- 16 S. Kumar, G. Gompper and R. Lipowsky, *Phys. Rev. Lett.*, 2001, **86**, 3911–3914.
- 17 J. Hu, T. Weikl and R. Lipowsky, *Soft Matter*, 2011, **7**, 6092–6102.
- 18 U. Seifert and R. Lipowsky, *Phys. Rev. A: At., Mol., Opt. Phys.*, 1990, **42**, 4768–4771.
- 19 R. Lipowsky, M. Brinkmann, R. Dimova, T. Franke, J. Kierfeld and X. Zhang, *J. Phys.: Condens. Matter*, 2005, **17**, S537–S558.
- 20 S. Komura, N. Shimokawa and D. Andelman, *Langmuir*, 2006, **22**, 6771–6774.
- 21 A. G. Ayuyan and F. S. Cohen, *Biophys. J.*, 2008, **94**, 2654–2666.
- 22 T. Hamada, Y. Kishimoto, T. Nagasaki and M. Tagaki, *Soft Matter*, 2011, **7**, 9061–9068.
- 23 T. Portet, S. E. Gordon and S. L. Keller, *Biophys. J.*, 2012, **103**, L35–L37.

- 24 W. Rawicz, K. C. Olbrich, T. McIntosh, D. Needham and E. Evans, *Biophys. J.*, 2000, **79**, 328–339.
- 25 K. J. Tierney, D. E. Block and M. L. Longo, *Biophys. J.*, 2005, **89**, 2481–2493.
- 26 R. Lipowsky, *Phys. Rev. Lett.*, 1996, **77**, 1652–1655.
- 27 T. Weikl and R. Lipowsky, *Phys. Rev. E: Stat., Nonlinear, Soft Matter Phys.*, 2001, **64**, 011903.
- 28 R. Lipowsky, *Faraday Discuss.*, 2013, **161**, 305–331.
- 29 C. Hofstätter, E. Lindahl and O. Edholm, *Biophys. J.*, 2003, **84**, 2192–2206.
- 30 O. Edholm and J. F. Nagle, *Biophys. J.*, 2005, **89**, 1827–1832.
- 31 M. Alwarawrah, J. Dai and J. Huang, *J. Phys. Chem.*, 2010, **114**, 7516–7523.
- 32 J. Pan, S. Tristram-Nagle and J. F. Nagle, *Phys. Rev. E: Stat., Nonlinear, Soft Matter Phys.*, 2009, **80**, 021931.
- 33 J. Gallova, D. Uhrikova, N. Kucerka, J. Teixeira and P. Balgavy, *Chem. Phys. Lipids*, 2010, **163**, 765–770.
- 34 D. A. Kofke and E. Glandt, *Mol. Phys.*, 1988, **64**, 1105–1131.
- 35 E. de Miguel, E. M. del Rio and M. M. T. da Gama, *J. Chem. Phys.*, 1995, **103**, 6188–6196.
- 36 Y. Tang, *J. Chem. Phys.*, 2012, **136**, 034505.
- 37 T. Gruhn, T. Franke, R. Dimova and R. Lipowsky, *Langmuir*, 2007, **23**, 5423–5429.
- 38 Y. Li, R. Lipowsky and R. Dimova, *Proc. Natl. Acad. Sci. U. S. A.*, 2011, **108**, 4731–4736.
- 39 J. Powles, W. Evans and N. Quirke, *Mol. Phys.*, 1982, **46**, 1347–1370.
- 40 J. G. Powles, *Chem. Phys. Lett.*, 1986, **125**, 113–117.
- 41 T. Fischer and R. L. C. Vink, *J. Chem. Phys.*, 2011, **134**, 055106.
- 42 J. Rowlinson and B. Widom, *Molecular Theory of Capillarity*, Clarendon Press, Oxford, 1989.
- 43 T. Baumgart, S. Hess and W. Webb, *Nature*, 2003, **425**, 821–824.
- 44 T. Baumgart, S. Das, W. W. Webb and J. T. Jenkins, *Biophys. J.*, 2005, **89**, 1067–1080.
- 45 S. Semrau, T. Idema, L. Holtzer, T. Schmidt and C. Storm, *Phys. Rev. Lett.*, 2008, **100**, 088101.
- 46 B. B. Machta, S. Papanikolaou, J. P. Sethna and S. L. Veatch, *Biophys. J.*, 2011, **134**, 1668–1677.
- 47 T. R. Weikl and R. Lipowsky, *Biophys. J.*, 2004, **87**, 3665–3678.
- 48 S. Safou and J. L. Thomas, *Biosens. Bioelectron.*, 2003, **18**, 445–455.
- 49 P. M. Bendix, M. S. Pedersen and D. Stamou, *Proc. Natl. Acad. Sci. U. S. A.*, 2009, **106**, 12341–12346.
- 50 I. Reviakine, M. Gallego, D. Johannesmann and E. Tellechea, *J. Chem. Phys.*, 2012, **136**, 084702.
- 51 M. Kocun, T. D. Lazzara, C. Steinem and A. Janshoff, *Langmuir*, 2011, **27**, 7672–7680.
- 52 T. M. Bayerl and M. Bloom, *Biophys. J.*, 1990, **58**, 357–362.